FT-IR detection of DMMP on TiO 2 -Modified Porous Silicon Substrates

Warda Raiah, M. Guendouz, Parastesh Pirasteh, Vincent Thomy, Joël Charrier, Yannick Coffinier

Materials Today Chemistry 42 (2024) 102363

Contents lists available at ScienceDirect

Materials Today Chemistry

journal homepage: www.journals.elsevier.com/materials-today-chemistry/

FT-IR detection of DMMP on TiO_2-Modified porous silicon substrates

Warda Raiah [a,b], Mohammed Guendouz [b], Parastesh Pirasteh [b], Vincent Thomy [a], Joël Charrier [b], Yannick Coffinier [a,*]

[a] Institut d'Electronique, de Microélectronique et de Nanotechnologie (IEMN, UMR CNRS 8520), Avenue Poincaré, BP 60069, 59652, Villeneuve d'Ascq, France
[b] Institut FOTON (UMR-CNRS 6082) Univ Rennes, 6 rue de Kérampont, 22305, Lannion, France

ARTICLE INFO

Keywords:
Porous silicon
Dimethyl methyl phosphonate
Titanium oxide
FT-IR
Gas sensor

ABSTRACT

In this study, we present a new chemical sensor based on a functionalized porous silicon and sensitive to dimethyl methyl phosphonate (DMMP), a simulant of sarin gas, known as one of the most toxic warfare agents. The porous silicon was prepared by anodising a boron-doped p-Si (100) wafer. A metal oxide TiO_2 layer was then deposited by thermal evaporation of Ti and oxidized under atmospheric conditions to form a TiO_2 film which was used as a reactive coating. The characterization of the PSi and TiO_2/PSi films was investigated using SEM, EDX and XPS spectroscopies. The results indicated that the TiO_2 was well incorporated on the surface and slightly inside the porous silicon layer. FT-IR studies were then carried out before and after exposure to DMMP and the detection performance was compared with PSi. The results obtained showed that our surfaces have the ability to detect DMMP down to 0.5 ppm compared to uncoated PSi layer. We have also shown that a TFA pre-treatment of our TiO_2 modified PSi, prior the exposure to DMMP, is crucial for increasing its sensitivity and that our sensor can be reused several times with a simple hexane cleaning step, a key criterion for routine applications.

1. Introduction

Today, as in the past, all living things, including animals and plants, are threatened by chemical warfare agents (CWAs). These synthetic chemical substances are known for their ability to cause immediate incapacitation, sudden death and permanent adverse health effects in humans and animals [1,2]. The use of these agents dates back to 600 BC with the contamination of water supplies by the Athenians and the production of toxic fumes in 429 BC [3]. Subsequently, after the Second World Wars, CWAs were used intermittently during the Iran-Iraq war in the 1980s [4], the Tokyo subway terrorist attacks in 1995 with 13 people dead and 6300 injured [5], in the conflict in Syria [6] and, more recently, the suspected poisoning of Sergei Skripal (ex-FSB agent) and his daughter and of Alexei Navalny, all by Novichok [7]. Indeed, nerve agents are among the most lethal weapons of mass destruction and are likely to be used by terrorists in attacks against civilians [5]. Many different types of CWAs, including nerve agents, blister agents, blood agents and incapacitating agents exist [1]. Most of these agents contain organophosphorus compounds and are among the most toxic substances, causing muscle contractions, convulsions, miosis and eventual death at low levels of exposure [8,9]. Because of their high toxicity and very limited use, studies of their environmental fate are often conducted using simulants [10]. Consequently, these simulants have been developed to mimic the relevant chemical and physical properties of the agent without the associated toxicological properties [11]. One of the simulants of the neurotoxic gas "sarin" is dimethyl methyl phosphonate DMMP. Sarin is classified as a chemical weapon of mass destruction because of its severe effects on the human health system, which can lead to neuromuscular paralysis or death, and because it is colourless and odourless [12]. The structures of sarin and its simulant DMMP are shown in Fig. 1.

DMMP is a commonly used simulant due to its stable properties, which are due to the presence of methyl methylphosphonate, which is stable even at higher temperatures up to 400 °C [13]. For this reason, it is also used as flame retardant additive [14]. In addition, this simulant has a chemical structure that includes the coordination of phosphorus to oxygen through a double bond -P═O and through single bonds -P-O-, which are very important to provide a reference and a basis for establishing an effective method to detect the real nerve agent sarin [15]. To date, several existing methods and sensors have been investigated for the detection of DMMP gases and related compounds. Among the most investigated sensors are semiconducting metal oxide sensors and especially ZnO and SnO_2 the most investigated ones [16]. These sensors are one of the most advantageous groups of chemiresistive gas sensors

* Corresponding author.
E-mail address: yannick.coffinier@univ-lille.fr (Y. Coffinier).

https://doi.org/10.1016/j.mtchem.2024.102363
Received 30 May 2024; Received in revised form 20 August 2024; Accepted 17 October 2024
Available online 22 October 2024

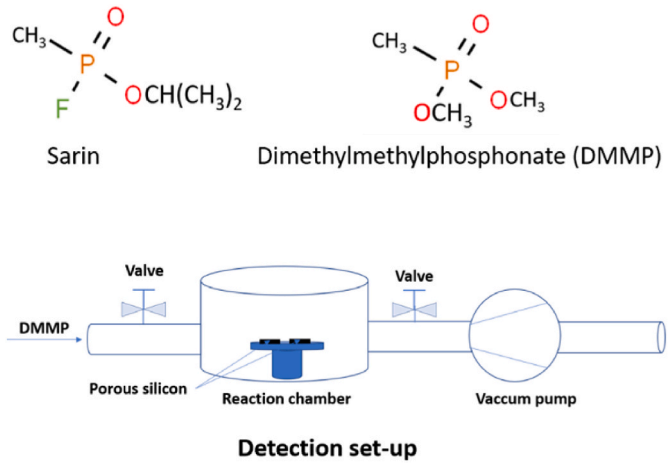

Fig. 1. The chemical structures of sarin and DMMP and the detection set-up.

compared to other types of sensors even if a recent study demonstrated the use of porous graphene for DMMP detection [17,18] However, other sensors exist that include quartz crystal microbalance (QCM) sensors [19] microcantilever-based (MCL) sensors [20] and surface acoustic wave (SAW) sensors [21]. The advantage of all these sensors lies in their cost, small size, high sensitivity and ease of fabrication [22]. To improve the performance of these sensors, we need to focus on two crucial points. The first one is the use of structures with large active surface area by using textures and porosities, for example. Porous silicon (PSi) has shown improved concentration limit of gas detection to a great extent. Such improvement is mainly the consequence of large surface to volume ratio of PSi [23,24]. Some reports described the detection of various gases like hydrogen, ammonia, oxygen, CO, CO_2, alcohol but also HF, hydrogen cyanide and diisopropyl fluorophosphate, a nerve agent, using PSi based gas sensors [25–29]. The second point is the implementation of reactive materials on PSi introducing a good affinity towards the molecules to be detected [30]. To this extent, several active materials have been proposed to improve the overall performance of these sensors. The use of CuO nanoparticles on micro-scale ZnO [31], cerium and iron oxides supported on alumina [32,33], alumina surface [34] and many others have been reported. However, Titanium dioxide (TiO_2) is still widely employed in particular in Metal Oxide Affinity Chromatography (MOAC) due to its high affinity for phosphate and phosphonate groups [35]. This characteristic makes TiO_2 an effective material for the selective enrichment and detection of phosphorylated compounds, which are critical in various biological and chemical processes [36]. Indeed, TiO_2 exhibits strong binding affinity and selectivity towards phosphate groups due to its surface properties and the ability to form stable complexes and has thus been used for the isolation of phosphorylated peptides and proteins from complex biological mixtures. It was, for example, notably applied in proteomics for the enrichment of phosphorylated proteins and peptides, facilitating the study of protein phosphorylation, a crucial post-translational modification that regulates many cellular processes [37]. TiO_2 is also utilized in environmental chemistry to detect, quantify and degrade phosphate and phosphonate-based pollutants (ex. Glyphosate) [38]. The use of TiO_2 in MOAC offers several advantages, including high binding capacity, robustness, and compatibility with various analytical techniques. Additionally, TiO_2 can be easily regenerated and reused, making it a cost-effective choice for repeated analyses. So, TiO_2-based metal oxide affinity chromatography is a powerful tool for the detection and analysis of phosphate and phosphonate-based compounds in relevant various samples. Its high affinity and selectivity for phosphorylated molecules make it essential in proteomics, forensics and environmental monitoring.

For the first time, we propose to use porous silicon (PSi) material combined to TiO_2 coating as the absorbing material for the detection of DMMP. PSi is widely used in the sensor domain and is known to be easy and inexpensive to produce. It is usually synthesised by electrochemical anodization. By adjusting the etching process, different nanostructures with different morphologies can be achieved thus influencing mainly its optical properties. Furthermore, another advantage of porous silicon is its high internal surface area (800 m^2/g). Based on previous reports on the addition of active materials that could improve DMMP detection capabilities, TiO_2 is one of a preferred choice [39]. In this context, the addition of TiO_2 coatings to PSi structures could enhance the adsorption performances of our sensor. To the best of our knowledge, this study is the first demonstration to date of the use of porous silicon for the DMMP detection. This work lies primarily in the use of TiO_2-coated PSi for the selective and sensitive detection of DMMP and the enhancement of sensitivity by TFA pre-treatment. The ability to reuse the sensor after cleaning is also novel, especially in the context of routine applications, which is a practical aspect of sensor reusability that is crucial for real-world applications. In addition, thanks to the ability of TiO_2 to interact with phosphorus-containing compounds, it makes it particularly effective and valuable for various applications such as in environmental monitoring, agricultural safety, and defense, where the rapid and reliable detection of toxic organophosphates is critical.

2. Experimental methods

2.1. Chemicals

DMMP and TFA were purchased from Alfa Aesar (97 %) and Sigma-Aldrich, respectively and both were used as received. Hydrofluoric acid (HF, 50 %) was purchased from Honeywell and acetone, dichloromethane (CH_2Cl_2), isopropyl alcohol, ethanol (EtOH) and hydrogen peroxide (30 %, w/w) were purchased from Carlo Erba. Ultrapure water (Milli-Q, 18 MΩ cm^{-1}) was used in the preparation of the solutions and in all rinsing steps when needed.

2.2. PSi fabrication

The PSi layers were obtained by electrochemical anodization of p-type doped (100) oriented silicon wafers (Resistivity 5.10^{-3} Ohm.cm) at room temperature. The electrolyte consisted of HF (50 %) in ethanol and deionized water in the following ratio 2:2:1. The refractive indices and porosities of PSi single layers were studied by reflectometry in the near and mid-infrared spectral region. From the reflectance spectra, the refractive index for each of the fabricated PSi single layers was deduced by fitting the experimental spectral fringes using the effective medium theory (Bruggeman model). The thickness of each porous layer was controlled by the anodising etching time. Current densities of 90 mA/cm^2 were used to obtain 80 % porosity. To open the pores, freshly prepared porous silicon was etched to remove a thin layer of low porosity using CHF_3 RIE - ICP plasma.

2.3. Scanning electron microscopy (SEM)

SEM technique was used to know the morphology and exact pores sizes of porous silicon layers before and after deposition of metal. The SEM images were obtained using an electron microscope ULTRA 55 (Zeiss, oberkochen Germany) equipped with a thermal field emission emitter, three different detectors (ESB detector with filter grid, high efficiency In-lens SE detector, Everhart-Thornley Secondary Electron Detector) and an energy dispersive X-ray analysis device (EDX analysis) (EDS Xflash 4010 system, Bruker, USA). Pore size distributions were calculated from the SEM images shown in Fig. 2 using ImageJ software.

2.4. Surface functionalization by TiO_2 film

PSi surfaces were then subjected to functionalization by deposition

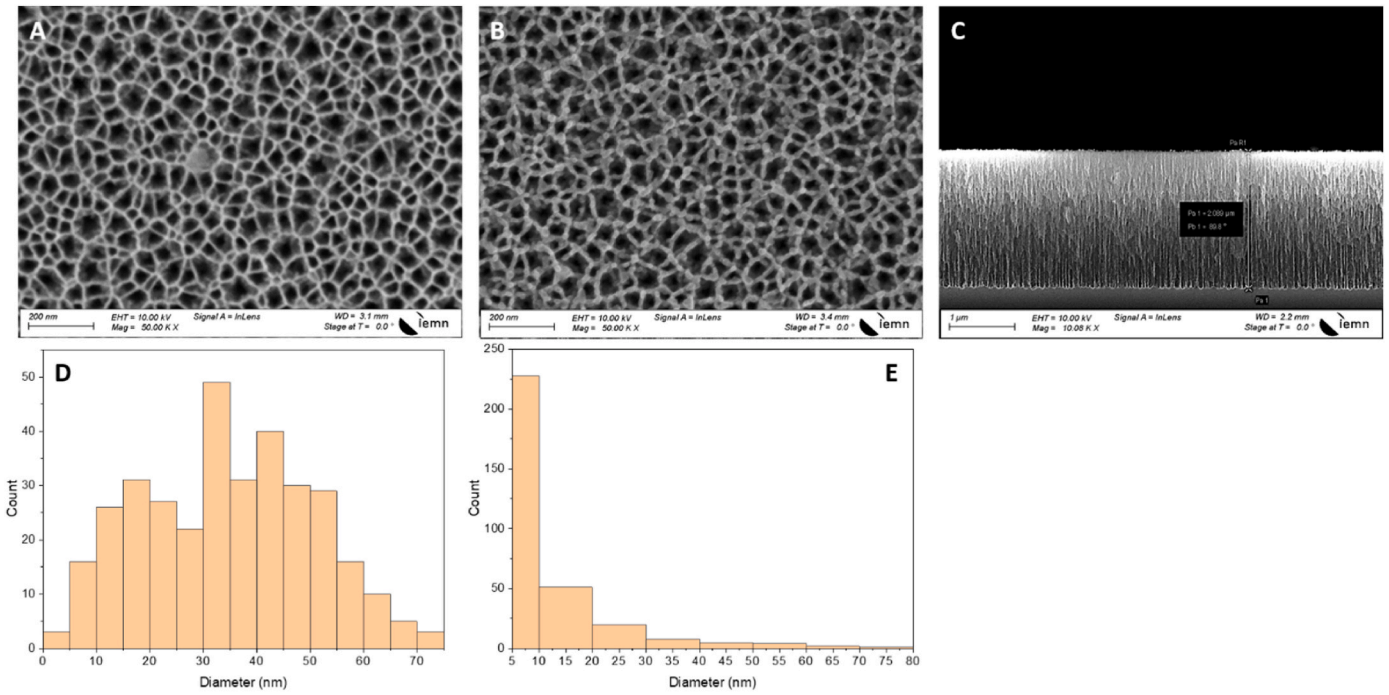

Fig. 2. Top-view SEM images of the 80 % porosity PSi layer before and after deposition of 10 nm of titanium (A, B), SEM cross-section image (C) and pore size distribution D (from SEM image A) and E (from SEM image B).

of titanium film using Physical vapour deposition (PVD) technique *via* thermal evaporation process. In our case, 10 nm of Ti was deposited using a PLASSYS MEB 500 device, equipped with quartz balance for checking the thickness of the deposited layer. Thanks to orbital rotation, homogeneity of the deposited layer is ensured. After that, Ti films were let oxidized in clean room facilities under ambient atmosphere for several hours prior its use. Finally, the functionalized surfaces were immersed in Trifluoroacetic acid for 15 s in order to promote the protonation of TiO_2 films and the introduction of positive charge before interaction with DMMP.

2.5. Measurement of water contact angle (WCA)

Water contact angles values were measured using deionized water as liquid test and a DIGIDROP goniometer system (GBX, France), with accuracy of ±2°. All measurements were made in the ambient atmosphere at room temperature on three different locations over each surface.

2.6. Fourier-transform infrared (FT-IR) spectroscopy

Specular reflection FT-IR spectra were recorded using an Thermo Scientific Nicolet 6700 FT-IR spectrometer This spectrometer analysis was performed in the wavenumber range from 400 cm^{-1} to 4000 cm^{-1}. All measurements were made after purging the sample chamber for 30 min with dry N_2. Spectra were recorded at 4 cm^{-1} spectral resolution and averaged over 200 scans. Background spectra were obtained using a flat untreated PSi surface. For each experimental conditions, the number of surface tested N = 3 and the number of tests by surface n = 3. Limit of detection and limit of quantitation were calculated based on the standard deviation of the response of the curve (SD) and the slope of the linear dynamic range curve (S) as follow: LoD= (3.3*(SD/S)) and LoQ (10*(SD/S)).

2.7. X-ray photoelectron spectroscopy (XPS)

XPS measurements were performed with an ESCALAB 220 XL spectrometer from Vacuum Generators. A monochromatic Al Kα X-ray source (1486.6 eV) was operated in constant analyser energy (CAE) mode (CAE = 100 eV for survey spectra and CAE = 40 eV for high resolution spectra) using the electromagnetic lens mode. The angle between the incident X-rays and the analyser is 58°. The detection angle of the photoelectrons is 90° relative to the sample surface and the C_{1s} at 285 eV was used for binding energy correction.

2.8. DMMP interaction

For the interaction of vapour of DMMP with PSi, we used a PELCO® Mini Hot Vac vacuum desiccator system (Fig. 1). This system consists of an aluminium base placed on a hot plate. The temperature of the plate is adjustable and can be heat up to 300 °C, which makes it easy to obtain gas vapours from the liquid state under a soda-lime glass bell. Perfect sealing and total isolation from any external contamination is guaranteed by the use of a silicone O-ring seal between the aluminium base and the glass dome and the use of a VRI-2 Rotary Pump Kit 55 for #2245 Vacuum Desiccator. This pump is connected to our system *via* a three-way valve, one to draw in the vacuum, the second to maintain it and the third to break the vacuum and stop the operation. In this study, we used different amounts of DMMP ranging from 2 to 135 ppm. The heating plate was set at 70 °C and the temperature of the heating plate was controlled by a digital thermometer included in the system. The interaction between porous silicon surfaces and DMMP vapour in this system was set over a period of 2 h and under a static vacuum fixed at 10^{-2} mbar. After the DMMP exposure, FT-IR spectroscopy measurement was performed.

2.9. Cleaning and regeneration of surfaces

A suitable cleaning process is one of the key steps to regenerate the active surface for its potential reuse in sensing applications. In this regard, several cleaning procedures were tested to remove DMMP residues from TiO_2–PSi. The first was to rinse the surfaces with hexane. In this case, the PSi and TiO_2/PSi surfaces were immersed in hexane for 10 s at room temperature. The surfaces were then rinsed with ethanol and dried

with a stream of N_2. The second procedure consists of a UV-Ozone cleaning process where the surfaces were kept in a Jelight 42 UVO Cleaner for various times with a maximum of 1h30. The third process was Plasma O_2 cleaning. In this case, the surfaces were placed in a plasma chamber (Oxford Plasmalab 80 Plus RIE system) and the following experimental conditions were applied: power 150 W, 20 sccm O_2, chamber pressure 100 mbar for two periods of 1 min each. After cleaning the surfaces using these techniques, the FT-IR spectrum of the functionalized PSi was recorded to evaluate the effectiveness of each cleaning method. In addition, to test the reusability of our sensor surfaces after cleaning, the FT-IR spectrum was recorded for each surface after interaction with DMMP vapour and after cleaning the surfaces using these different cleaning procedures.

3. Results and discussion

The PSi layers were fabricated through electrochemical anodization of p-type doped (100)-oriented silicon wafers (5.10^{-3} Ω cm^{-1}) at room temperature, using an electrolyte mixture of HF, deionized water, and ethanol in a 2:1:2 ratio. Electrochemical anodization allows precise control over the direction of pore formation in bulk silicon by selecting the doping type and level of the initial silicon material. The thickness of the PSi layer was determined by the anodization etching duration, while a current density of 90 mA/cm^2 was applied to achieve 80 % porosity. Fig. 2 presents SEM images of PSi before and after Ti deposition. The resulting structures are primarily columnar, characteristic of mesoporous silicon, with PSi single layer featuring pore diameters between 20 and 60 nm and homogeneous layer thickness of 2 μm (Fig. 2C). Post Ti deposition, as seen in Fig. 2B, shows that there is a significant change in surface morphology, exhibiting thicker pore walls and a grain-like texture due to the Ti deposition. Despite these changes, the pores remain open, although their diameters are now reduced to a range of 10–30 nm. The calculation of the pore size distribution using ImageJ from the SEM image shown in Fig. 2D confirms this point. Indeed, for unmodified PSi, a pore size distribution centred around 30 nm is observed, whereas for TiO_2–PSi a strong decrease to lower dimensions was calculated after metallisation, with the majority of the distribution below 20 nm (Fig. 2E). It is clear that metallisation has significantly reduced the pore diameter compared to unmodified PSi.

When titanium is exposed to the atmosphere, it reacts rapidly with oxygen to form titanium dioxide (TiO_2). The formation of this oxide layer begins immediately upon exposure to air, as titanium has a strong affinity for oxygen. The initial oxide layer is typically around 1–2 nm thick, but can become thicker over time, reaching up to 25 nm under ambient conditions. In addition, the titanium dioxide layer formed during atmospheric oxidation is highly stable and strongly adheres to the underlying surface. Here, we have examined the surface chemistry of PSi after Ti film deposition to ensure the presence of the TiO_2 layer. Fig. 3 shows the EDX spectrum of the PSi layer after deposition of 10 nm of Ti. We can observe the presence of Si, O and Ti. It should be noted that the O signal comes from both native oxide Si and TiO_2 layers. In addition, the high resolution Ti_{2p} XPS spectrum shows characteristic peaks' position corresponding to the TiO_2 layer. Indeed, Ti_{2p} 1/2 and 3/2 are located at binding energies of 465.19 and 459.41 eV, respectively, with a spin-orbital splitting of 5.8 eV typical of TiO_2 layers. For comparison, metallic Ti (0) has a Ti_{2p} 3/2 binding energy of 453.9 eV and a spin-orbit splitting of 6.1 eV. In addition, the ratio of Ti/O of the TiO_2 film is 0.30 compared to classical TiO_2 stoichiometry that presents a theoretical Ti/O ratio of 0.5. This is in good accordance with our previous study [36]. It has to be noted that since the coverage of PSi by thermal evaporation of Ti is not conformal as compared to ALD deposition technique, we cannot neglect oxygen contribution from native silicon oxide. All of this proves that we have a TiO_2 layer on the PSi surface. The wetting properties of the PSi surfaces before and after functionalization were also evaluated using static contact angle measurements (Table 1). We can observe that the freshly prepared PSi layer exhibits a moderate hydrophobic character with a water contact angle of 80° due to the residual presence of fluorine (from HF) after anodization. However, after the deposition of Ti film and its atmospheric oxidation, the contact angle decreased to 13° displaying a hydrophilic character due to the presence of TiO_2 layer.

Titanium dioxide (TiO_2) is a versatile material widely used in various applications due to its excellent photocatalytic properties, chemical stability, and high surface area [40]. One of the areas where TiO_2 has garnered significant interest is in the detection and degradation of chemical warfare agents (CWAs) and their simulants. As shown above, Dimethyl methylphosphonate (DMMP) is a common simulant for nerve agents such as sarin and soman. It is well known that DMMP molecules adsorb onto the surface of TiO_2. The adsorption can occur through various mechanisms, including physisorption (weak Van der Waals forces) and chemisorption (stronger chemical bonds) [41]. The nature and extent of adsorption depend on factors such as the surface area,

Table 1
Water contact angles for PSi and TiO_2–PSi surfaces.

Porous Si surfaces	WCA (°)
PSi freshly prepared	**80 ± 4**
PSi–TiO_2	**13 ± 2**
PSi + TFA treatment	**8 ± 1**
PSi–TiO_2 + TFA treatment	**5 ± 1**
PSi + DMMP	**17 ± 2**
PSi–TiO_2 + DMMP	**26 ± 3**

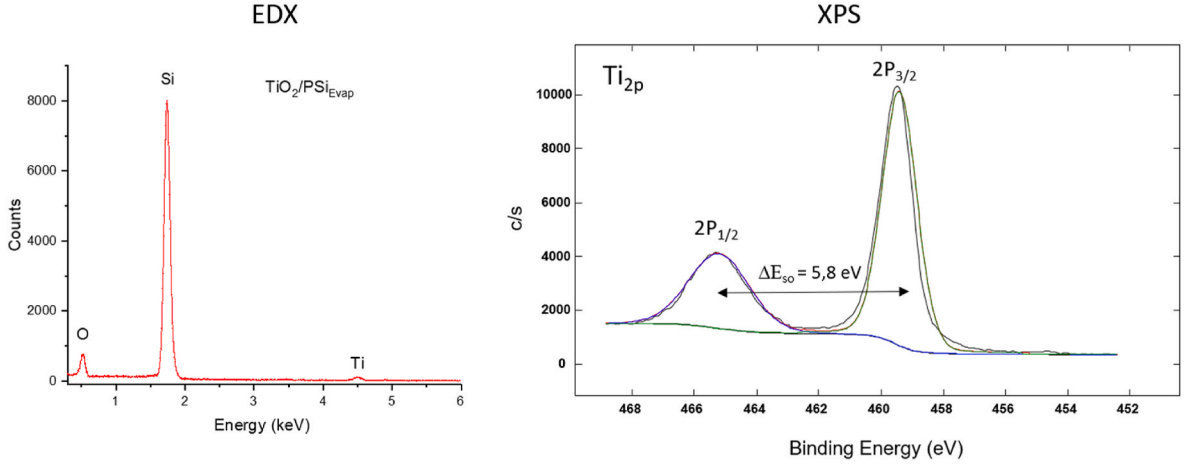

Fig. 3. EDX spectrum of TiO_2–PSi surface (left) and the high resolution XPS spectrum of Ti_{2P} (right).

crystallinity, and surface functional groups of the TiO_2. The huge surface area of porous silicon layer may enhance adsorption capacity of DMMP. Both of these hallmarks make this functionalized surface very interesting for such detection. After the characterization of our TiO_2–PSi surface, they were submitted to various amount of DMMP vapour during 2 h. To do so, we have considered a static and under vacuum modes @room temperature (DMMP was vaporized at 70 °C prior its injection in the interaction chamber (see Fig. 1 for the set-up)). Heating DMMP at 70 °C is expected to favour its vaporization. Various amounts of pure DMMP (ranging from 2 to 135 ppm) were used. After each exposure, FT-IR measurements were performed. As a reference surface, we used un-modified PSi surface. In Fig. 4A are displayed FT-IR spectra of DMMP detection after its interaction with TiO_2–PSi and PSi surfaces. Two characteristic peaks at 1315 and 1266 cm^{-1} were present due to the symmetric deformation mode of P–CH_3 and to P═O stretching centred, respectively [42,43]. These two peaks were present on both surfaces but with high signal intensities for TiO_2–PSi compared to PSi (8 times more intense) that showed a better affinity of DMMP for TiO_2 coating as expected.

Titanium oxide (TiO_2) possesses amphoteric properties, enabling it to act as either a Lewis acid or a Lewis base depending on the pH of its environment. In that case, DMMP molecules are either involved in Lewis acid-base interactions such as P═O···M or in hydrogen bonding interactions between the P═O group from DMMP and hydroxyl groups –OH from the surface [44]. For instance, under acidic conditions, TiO_2 functions as a Lewis acid with positive charges thus exhibiting ion-exchange characteristics. In the contrary, under more alkaline conditions, TiO_2 presents negative charge due to its deprotonation. The interaction mechanism involves both ion exchange and Lewis acid/base interactions, resulting in high specificity. To enhance the detection performances of our surface, we have immerged our TiO_2–PSi surface in a TFA solution (0.1 %, pH 3) during 5 s prior its interaction with DMMP. In Fig. 4**B** are displayed FT-IR spectra of TiO_2–PSi layers w/o TFA pre-treatment prior exposure to DMMP. We can observe that the 2 characteristic peaks at 1262 and 1315 cm^{-1} are present in both cases but with higher intensity for P═O stretching (3 times more) in the case of TFA treated TiO_2–PSi surface. Thus, it seems that TFA treatment enhances the interaction between P═O and TiO_2 coating. For further experiments, we kept this pre-treatment. In addition, in Fig. 4C is displayed the high resolution XPS spectrum of P_{2p} obtained on TiO_2–PSi surface after its exposure to 4 ppm of DMMP. The inter (N = 3) and intra (n = 3) standard deviations are 20 % and 1.4 % respectively. The moderately good inter-surface standard deviation could be explained by the homogeneity issue of the porosity of PSi between the different anodising batches. One solution will be to process a 3 inches Si wafer and then dice it into smaller chips.

In the following section, we have carried out experiments to determine the sensing linear dynamic range of our TiO_2–PSi surface, which provides valuable insights in terms of sensitivity, together with improving the effectiveness and reliability of the sensor performance. It also helps us to determine the saturation point of the sensor, ensuring accurate measurements over a range of gas concentrations. Different amounts of DMMP ranging from 2 to 135 ppm were injected into the reaction chamber under the experimental conditions described above. FT-IR spectroscopic characterisation was then carried out. In Fig. 5 are displayed the signal intensities (area of the peak) for both P═O and P–CH_3 vibration modes in function of the DMMP concentration. We can see that for both signal intensities, our sensors reach saturation after 10

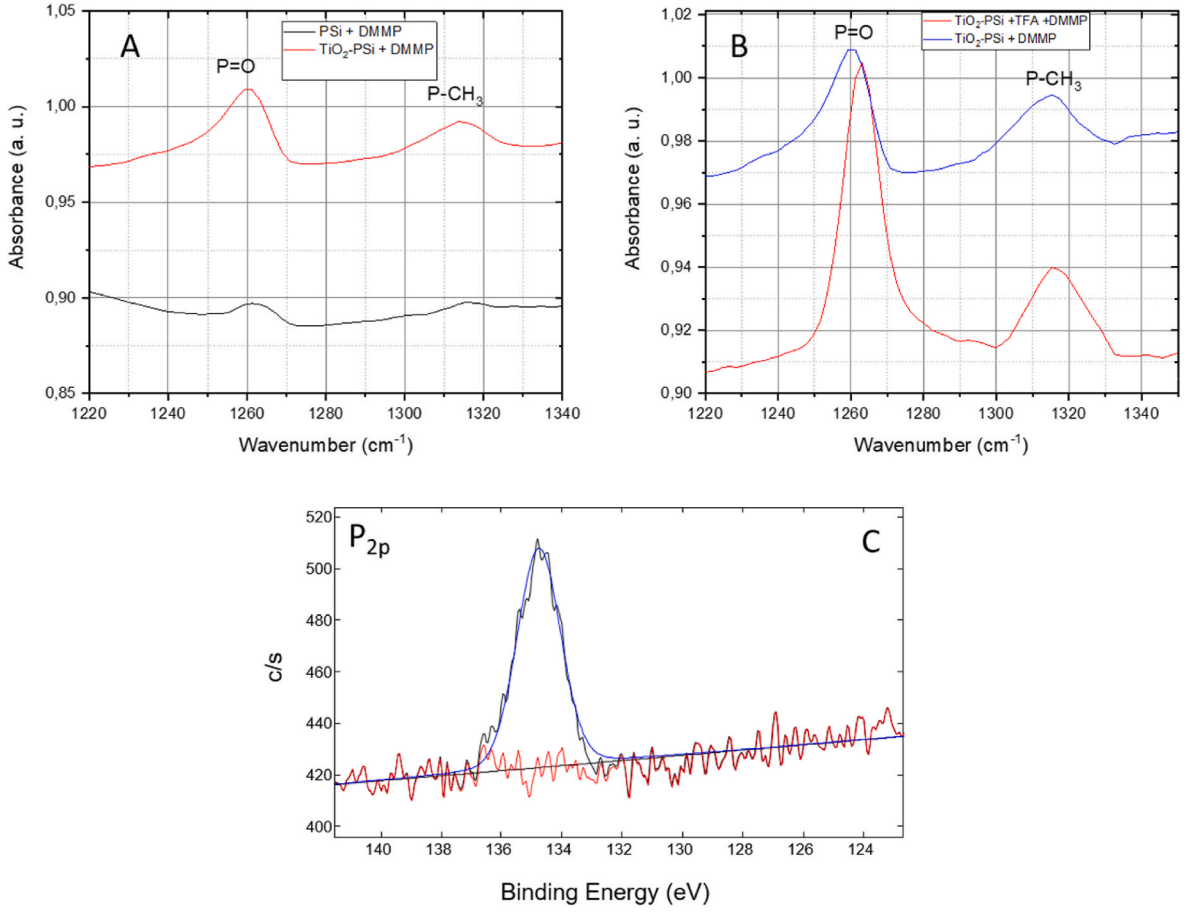

Fig. 4. Reflectance-mode FT-IR spectra of PSi and TiO_2–PSi after exposition to DMMP vapour (A), impact of TFA TiO_2–PSi pre-treatment on signal FT-IR intensity (B) and high resolution P_{2p} XPS spectrum from TiO_2–PSi surface after 4 ppm DMMP exposition (C).

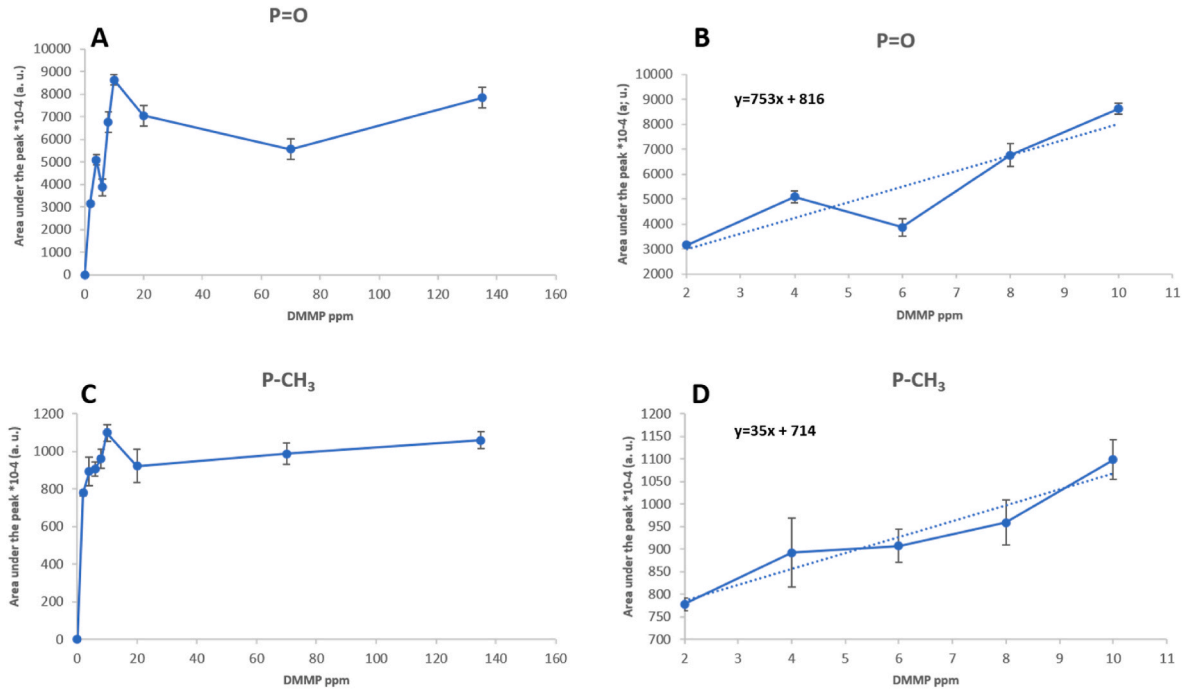

Fig. 5. Peak intensities for both P═O and P–CH_3 from FT-IR characterization on TiO_2–PSi surface after exposure to different amounts of DMMP (from 2 to 135 ppm). (N = 3 and n = 3). Figures B and D correspond to the intensities obtained between 2 and 10 ppm of DMMP for P═O and P–CH_3, respectively.

ppm DMMP. A drop in the intensities of the P═O and P–CH_3 signals is observed at 20 ppm and for higher DMMP concentrations. This can be explained by the saturation of the reactive groups on TiO_2 and the inhibition of its interaction with DMMP at higher concentrations. However, for DMMP levels between 2 and 10 ppm, we observe a good linear dynamic range, which defines the working range of our sensor, making it possible to carry out semi-quantitative or even quantitative measurements with LoD and LoQ values (P═O) of 0.5 and 5 ppm, respectively and $R^2 = 0.92$. However, using a different approach such as depositing a conformal TiO_2 layer by ALD deposition could be a good option to improve the sensitivity of DMMP detection. In addition, PSi membrane could also be used instead to allow better gas perfusion through the porous cavities and then exploit all the surface area to enhance the sensitivity [45].

Reusable gas sensors represent a significant advance in environmental monitoring, industrial safety and public health. The development and implementation of such sensors offer several key advantages, including cost effectiveness. Indeed, reusable sensors reduce the overall cost of gas detection systems. Instead of having to replace disposable sensors frequently, reusable sensors can be regenerated and reused many times, resulting in long-term savings and lower operating costs. Secondly, the use of reusable sensors contributes to more sustainable environmental practices, particularly by reducing the number of sensors discarded after each use; the environmental footprint of gas sensing operations is significantly reduced, and the lower replacement costs translate into significant financial savings. Thirdly, reusable sensors are often designed with robust materials and advanced technologies, ensuring greater reliability and consistent performance over time. This reliability is critical in applications such as industrial safety, forensics and environmental monitoring where accurate and continuous gas detection is essential. In addition, more consistent and reliable data can be expected over time. Reusable sensors maintain data continuity, which is particularly important in long-term monitoring applications where data integrity is mandatory. Finally, the ability to regenerate and reuse sensing faces simplifies the maintenance and management of gas sensing systems. This convenience can reduce downtime and promote more efficient operations, as sensors can be quickly restored to optimum performance without the need for frequent replacement. To this end, and to evaluate the reusability of the TiO_2–PSi sensor surface, we tested 3 different cleaning procedures after exposure to DMMP. The effectiveness of the cleaning step was assessed by the disappearance of the 2 characteristic peaks at 1262 and 1315 cm^{-1} by FT-IR. To do so, we first submitted the TiO_2–PSi surface, after its exposure to DMMP, to Plasma O_2 cleaning. In that case, the surfaces were placed in a plasma chamber (Oxford Plasmalab 80 Plus RIE system) and the following experimental conditions were applied: power 150 W, 20 sccm O_2, chamber pressure 100 mbar for two periods of 1 min each. The results showed that the absorption band characteristic of the P–CH_3 bond is completely eliminated after 120 s of plasma O_2 treatment. However, this treatment did not completely eliminate the P═O bonds with only 66 % removed after 1 min and 88 % after the second period of 1 min compared to the initial peak intensity (Fig. 6A). We can also observe that the peak position of P═O was shifted to 1278 cm^{-1}. This significant shift in the P═O stretching mode is observed in other phosphonic esters and is attributed to the environmental sensitivity of the phosphoryl (P═O) stretching mode that could be significantly perturbed upon adsorption [46]. Crooks et al., proposed 2 modes of interaction of the DMMP adsorbed on the TiO_2 surface. In the first mode, the oxygen of the phosphoryl group is hydrogen bonded to the hydroxylated TiO_2 surface while in the second structure the electron-rich phosphoryl oxygen forms an adduct with a Lewis acid (Ti^{4+}, Ti^{3+}) site [44]. The plasma O_2 treatment can also change the surface chemistry of TiO_2, introducing other oxygen species that can interact differently with DMMP. Finally, we cannot exclude the DMMP degradation upon plasma O_2 treatment that could lead to a drastic conversion of DMMP to phosphate and other products that could explain the shift of the P═O peak position [47].

For the second cleaning procedure, we used UV ozone treatment, which was effective in removing the DMMP molecule from the surface of the TiO_2–PSi surface, but only after three consecutive treatments of 30 min each (Fig. 6B). Indeed, while the peak corresponding to P–CH_3 has completely disappeared after 30 min as shown in Fig. 6B, the P═O peak (1263 cm^{-1}) has lost only 76 % of its intensity compared to the initial peak after the first 30 min of UV ozone treatment and 90–95 % after the second and third treatments (90 min in total), respectively. Here, the

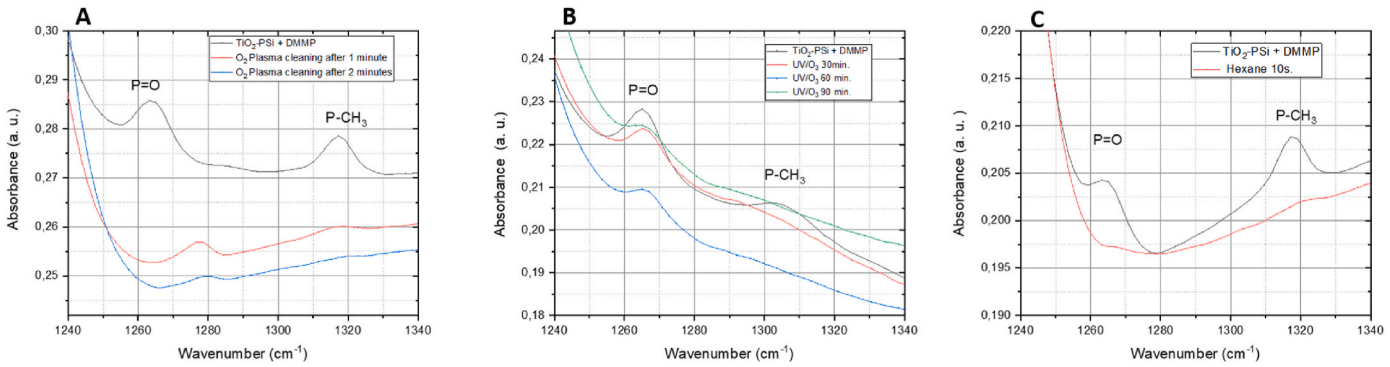

Fig. 6. FT-IR spectra of TiO_2–PSi surface after exposure to DMMP before and after cleaning with A) O_2 plasma treatment, B) UV/O_3 treatment and C) with hexane treatment.

effectiveness of the cleaning is mainly due to the photocatalytic properties of TiO_2, as it is known to be an efficient photocatalyst for the photodegradation of DMMP under UV illumination [48].

For the last cleaning procedure, we chose to immerse the TiO_2–PSi surface after exposure to DMMP in a hexane solution for 10 s at room temperature, then rinse the surface with ethanol and dry it with a stream of N_2. Surprisingly, the FT-IR measurements, in Fig. 6C, show the disappearance of the two characteristic peaks P–CH_3 and P═O after a single immersion in hexane solution. It has been shown that TiO_2 materials contaminated by methylphosphonic acid (MPA) and PO_4^{3-} products from DMMP photodegradation can be washed away by H_2O [49]. In our case, a simple rinse with hexane may be sufficient to remove DMMP and related products. From all these experiments, the hexane cleaning procedure was selected for its efficiency, low cost, simplicity and speed of use.

Based on this, we wanted to demonstrate that our TiO_2–PSi surface can be used several times for the detection of DMMP without losing its performance. To do this, a hexane rinse was performed between each test. In Fig. 7, we can see that the signal for P═O and P–CH_3 disappeared after each rinsing step. In addition, for each test with DMMP, the signal intensity for both P═O and P–CH_3 are observed, showing the ability to reuse the same surface several times without losing the detection performance.

The threshold level of exposure, known as the immediately dangerous for life or health limit (IDLH), represents the concentration of a chemical in the air that can cause immediate or delayed permanent adverse health effects after 30 min of unprotected exposure. For malathion and parathion, two commonly used organophosphorus pesticides, the IDLH values are 18.52 ppm and 0.84 ppm, respectively. In contrast, the IDLH limits for chemical warfare agents are much lower, at approximately 0.03 ppm for sarin, 0.008 ppm for soman, and 0.03 ppm for tabun [42]. Thus, we can see that the detection performance of our TiO_2–PSi nanomaterials is in line with the IDLH limits for some pesticides, but underperforms for the detection of warfare agents. However, currently none of the available OP detection techniques fully meet all the necessary requirements for simultaneous high sensitivity, selectivity, portability and fast response time at these IDLH limits. In the near future, we believe that our nanomaterials could be of interest by combining FT-IR spectroscopy and mass spectrometry techniques. Indeed, we have already shown that TiO_2-modified nanowires could be used as an inorganic matrix for LDI-MS detection of phosphorylated peptides [36]. Thus, the combination of FT-IR spectroscopy and ion mobility mass spectrometry (IMS) could have a synergistic effect and improve the overall ability to detect and identify CWAs. It should be noted that IMS is already being used at airports to accurately detect and identify explosives and common illicit drugs in less than 8 s (https://www.smithsdetection.com/products/ionscan-600/). Each technique will provide unique information about the chemical structure and properties of CWAs, leading to more accurate identification. In addition, the integration of portable versions of these technologies will allow rapid on-site detection, which is critical in emergency situations [50].

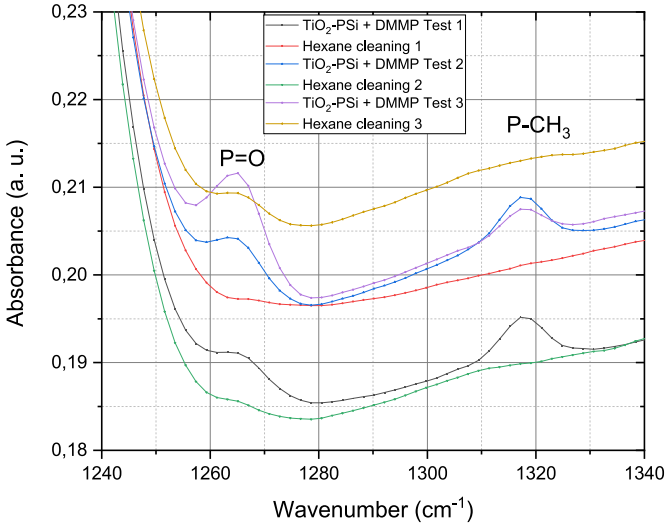

Fig. 7. FT-IR spectra obtained from 3 consecutive tests of the TiO_2–PSi surface after exposure to DMMP (4 ppm), with a hexane cleaning step between each test.

4. Conclusion

In this paper, we have shown that the modification of PSi surface by TiO_2 coating *via* thermal evaporation of Ti film and followed by its atmospheric oxidation can be used for the detection of DMMP vapour. After characterisation of the functionalized PSi by SEM, EDX, WCA and XPS analyses, the detection of DMMP was performed by FT-IR spectroscopy. We have shown that the presence of TiO_2 confers a certain selectivity towards DMMP compared to unmodified PSi. We have demonstrated that the pre-treatment of the TiO_2–PSi surface with TFA solution enhances the signal intensity of the P═O vibrational mode by promoting the Lewis acid interaction. Then, we found a linear dynamic range of the sensor between 2 and 10 ppm with a LoD of 0.5 ppm which opens the possibility to perform quantitative measurements within this range of concentrations of DMMP. Finally, we presented a reusable surface thanks to an efficient, low-cost and fast cleaning step using hexane solution, giving the possibility to reuse our surface up to 3 times without any loss of sensing properties.

CRediT authorship contribution statement

Warda Raiah: Investigation, Formal analysis. **Mohammed**

Guendouz: Writing – review & editing, Supervision, Methodology, Investigation, Formal analysis, Conceptualization. **Parastesh Pirasteh:** Writing – review & editing, Methodology, Conceptualization. **Vincent Thomy:** Writing – review & editing, Supervision. **Joël Charrier:** Writing – review & editing, Supervision, Project administration, Funding acquisition, Conceptualization. **Yannick Coffinier:** Writing – review & editing, Writing – original draft, Validation, Supervision, Methodology, Investigation, Funding acquisition, Formal analysis, Data curation, Conceptualization.

Declaration of competing interest

The authors declare that they have no known competing financial interests or personal relationships that could have appeared to influence the work reported in this paper.

Acknowledgements

The authors acknowledge theFrench Agence Nationale de la Recherche (ANR) for financial support as part of the ANR MID-VOC project (ANR- 17-CE09-0028-01), the Centre National de la Recherche Scientifique (CNRS), the University of Lille and the University of Rennes. This work was partly supported by the French RENATECH network (French national nanofabrication platform) and the CMNF platform of IEMN.

Data availability

Data will be made available on request.

References

[1] F.N. Diauudin, J.I. Abdul Rashid, V.F. Knight, W.M. Zin Wan Yunus, K.K. Ong, N. A. Mohd Kasim, N.A. Halim, S.A. Mohd Noor, A review of current advances in the detection of organophosphorus chemical warfare agents-based biosensor approaches, Sens. Bio-Sens. Res. 26 (2019) 100305.
[2] V. Kumar, H. Kim, B. Pandey, T.D. James, J. Yoon, E.V. Anslyn, Recent advances in fluorescent and colorimetric chemosensors for the detection of chemical warfare agents: a legacy of the 21st century, Chem. Soc. Rev. 52 (2023) 663.
[3] S. Chauhan, S. Chauhan, R. D'Cruz, S. Faruqi, K.K. Singh, S. Varma, M. Singh, V. Karthik, Chemical warfare agents, Environ. Toxicol. Pharmacol. 26 (2008) 113.
[4] F.W. Dagnaw, W. Feng, Q.H. Song, Selective and rapid detection of nerve agent simulants by polymer fibers with a fluorescent chemosensor in gas phase, Sensor. Actuator. B Chem. 318 (2020) 127937.
[5] T. Okumura, N. Takasu, S. Ishimatsu, S. Miyanoki, A. Misuhashi, K. Kumada, K. Tanaka, S. Hinohara, Report on 640 Victims of the Tokyo subway sarin attack, Ann. Emerg. Med. 28 (1996) 129.
[6] S. Fan, G. Zhang, G.H. Dennison, N. FitzGerald, P.L. Burn, I.R. Gentle, P.E. Shaw, Challenges in fluorescence detection of chemical warfare agent vapors using solid-state films, Adv. Mater. 32 (2020) 1905785.
[7] https://www.independent.co.uk/news/uk/politics/sergei-andyulia-skripal-in-salisbury-attack-was-a-novichok-nerve-agentconfirms-chemical-weapons-watchdog-a8301121.html (December 2021).
[8] J. Wang, M.P. Chatrathi, A. Mulchandani, W. Chen, Capillary electrophoresis microchips for separation and detection of organophosphate nerve agents, Anal. Chem. 73 (2001) 1804.
[9] J.L.S. Sporty, S.W. Lemire, E.M. Jakubowski, J.A. Renner, R.A. Evans, R. F. Williams, J.G. Schmidt, M.J. van der Schans, D. Noort, R.C. Johnson, Immunomagnetic separation and quantification of Butyrylcholinesterase nerve agent adducts in human Serum, Anal. Chem. 82 (2010) 6593.
[10] G.W. Wagner, P.W. Bartram, Reactions of VX, HD, and their simulants with NaY and AgY Zeolites. Desulfurization of VX on AgY, Langmuir 15 (1999) 8113.
[11] B.C. Singer, A.T. Hodgson, H. Destaillats, T. Hotchi, K.L. Revzan, R.G. Sextro, Indoor sorption of surrogates for sarin and related nerve agents, Environ. Sci. Technol. 39 (2005) 3203.
[12] L.A. Patil, A.R. Bari, M.D. Shinde, V. Deo, M.P. Kaushik, Detection of dimethyl methyl phosphonate – a simulant of sarin: the highly toxic chemical warfare – using platinum activated nanocrystalline ZnO thick films, Sensor. Actuator. B Chem. 161 (2012) 372.
[13] S.C. Lee, H.Y. Choi, S.J. Lee, W.S. Lee, J.S. Huh, D.D. Lee, J.C. Kim, The development of SnO2-based recoverable gas sensors for the detection of DMMP, Sensor. Actuator. B Chem. 137 (2009) 239.
[14] H.F. Xiang, H.Y. Xu, Z.Z. Wang, C.H. Chen, Dimethyl methylphosphonate (DMMP) as an efficient flame-retardant additive for the lithium-ion battery electrolytes, J. Power Sources 173 (2007) 562.
[15] Q. Zheng, Y. Fu, J. Xu, Advances in the chemical sensors for the detection of DMMP - a simulant for nerve agent sarin, Procedia Eng. 7 (2010) 179.
[16] D. Barreca, C. Maccato, A. Gasparotto, Metal oxide nanosystems as chemoresistive gas sensors for chemical warfare agents: a focused review, Adv. Mater. Interfac. 9 (2022) 2102525.
[17] Z. Yang, L. Zhao, Y. Zhang, Y. Xing, T. Fei, S. Liu, T. Zhang, DMMP sensors based on Au-SnO2 hybrids prepared through colloidal assembly approach: gas sensing performances and mechanism study, Sensor. Actuator. B Chem. 369 (2022) 132278.
[18] Y. Wang, M. Yang, W. Liu, L. Dong, D. Chen, C. Peng, Gas sensors based on assembled porous graphene multilayer frameworks for DMMP detection, J. Mater. Chem. C 30 (2019) 9248.
[19] D. Chen, K. Zhang, H. Zhou, G. Fan, Y. Wang, G. Li, A wireless-electrodeless quartz crystal microbalance with dissipation DMMP sensor, Sensor. Actuator. B Chem. 261 (2018) 408.
[20] G. Zuo, X. Li, T. Yang, Y. Wang, Z. Cheng, S. Feng, Detection of trace organophosphorus vapor with a self-assembled bilayer functionalized SiO_2 microcantilever piezoresistive sensor, Anal. Chim. Acta 580 (2006) 123.
[21] S. Lama, J. Kim, S. Ramesh, Y.J. Lee, J. Kim, J.H. Kim, Highly sensitive hybrid nanostructures for dimethyl methyl phosphonate detection, Micromachines 12 (2021) 648.
[22] C. Yu, Q. Hao, S. Saha, L. Shi, X. Kong, Z. Wang, Integration of metal oxide nanobelts with microsystems for nerve agent detection, Appl. Phys. Lett. 86 (2005) 063101.
[23] N. Naderi, M.R. Hashim, T.S.T. Amran, Enhanced physical properties of porous silicon for improved hydrogen gas sensing, Superlattice. Microst. 51 (2012) 626.
[24] V.A. Moshnikov, I. Gracheva, A.S. Lenshin, Y.M. Spivak, M.G. Anchkov, V. V. Kuznetsov, J.M. Olchowik, Porous silicon with embedded metal oxides for gas sensing applications, J. Non-Cryst. Solids 358 (2012) 590.
[25] L. Canham, Handbook of porous silicon, Handb, Porous Silicon (2014) 1–1017.
[26] A.M. Alwan, H.R. Abed, R.B. Rashid, Enhancing the temporal response of modified porous silicon-based CO gas sensor, Solid State Electron. 181 (2021) 181108019.
[27] A.M. Alwan, H.R. Abed, A.A. Yousif, Effect of the deposition temperature on ammonia gas sensing based on SnO2/porous silicon, Plasmonics 16 (2021) 501–509.
[28] Y.S. Lu, S. Vijayakumar, A. Chaix, B.R. Pimentel, K.C. Bentz, S. Li, A. Chan, C. Wahl, J.S. Ha, D.E. Hunka, G.R. Boss, S.M. Cohen, M.J. Sailor, Remote detection of HCN, HF, and nerve agent vapors based on self-referencing, dye-impregnated porous silicon photonic crystals, ACS Sens. 6 (2021) 418.
[29] A. Ghaderi, J. Sabbaghzadeh, L. Dejam, G.B. Pour, E. Moghimi, R.S. Matos, H.D. da Fonseca Filho, S. Țălu, A.S. shayegan, L.F. Aval, M.A. Doudaran, A. Sari, S. Solaymani, Nanoscale morphology, optical dynamics and gas sensor of porous silicon, Scientifc Reports 14 (2024) 3677.
[30] X. Wang, X. Li, Q. Wu, Y. Yuan, W. Liu, C. Han, X. Wang, Detection of Dimethyl methyl phosphonate by by silica molecularly imprinted materials, Nanomaterials 13 (2023) 2871.
[31] R. Yoo, S. Yoo, D. Lee, J. Kim, S. Cho, W. Lee, Highly selective detection of dimethyl methylphosphonate (DMMP) using CuO nanoparticles/ZnO flowers heterojunction, Sensor. Actuator. B Chem. 240 (2017) 1099.
[32] M.B. Mitchell, V.N. Sheinker, A.B. Tesfamichael, E.N. Gatimu, M. Nunley, Decomposition of dimethyl methylphosphonate (DMMP) on supported cerium and iron Co-impregnated oxides at room temperature, J. Phys. Chem. B 107 (2003) 580.
[33] M.B. Mitchell, V.N. Sheinker, W.W. Cox, E.N. Gatimu, A.B. Tesfamichael, The room temperature decomposition mechanism of dimethyl methylphosphonate (DMMP) on alumina-supported cerium oxide - participation of nano-sized cerium oxide domains, J. Phys. Chem. B 108 (2004) 1634.
[34] M.K. Templeton, W.H. Weinberg, Adsorption and decomposition of dimethyl methylphosphonate on an aluminum oxide surface, J. Am. Chem. Soc. 107 (1985) 97.
[35] M.R. Larsen, M.R. Thingholm, T.E. Jensen, O.N. Roepstorff, P. Jorgensen, T. J. Highly, Selective enrichment of phosphorylated peptides from peptide mixtures using titanium dioxide microcolumns, Mol. Cell. Proteomics 4 (2005) 4–873.
[36] I. Kurylo, A. Hamdi, A. Addad, R. Boukherroub, Y. Coffinier, Comparison of Ti based coatings on silicon nanowires for phosphopeptides' enrichment and their laser assisted desorption/ionization mass spectrometry detection, Nanomaterials 7 (2017) 272–291.
[37] T.E. Thingholm, O.N. Jensen, M.R. Larsen, Analytical strategies for phosphoproteomics, Proteomics 9 (2009) 1451.
[38] S.M. Ilina, P. Olivier, D.S. Lomberg, N. Baran, A. Pariat, N. Devau, N. Sanikast, M. Scheringer, J. Labille, Investigations into titanium dioxide nanoparticle and pesticide interactions in aqueous environments, Environ. Sci.: Nano 10 (2017) 2055.
[39] U. Biapo, A. Ghisolfi, G. Gerer, D. Spitzer, V. Keller, T. Cottineau, Functionalized TiO_2 nanorods on a microcantilever for the detection of organophosphorus chemical agents in air, ACS Appl. Mater. Interfaces 11 (2019) 35122.
[40] K. Solymos, I. Babcsányi, B. Ariya, T. Gyulavári, Á. Ágoston, Á. Szamosvölgyi, Á. Kukovecz, Z. Kónya, A. Farsang, Z. Pap, Photocatalytic and surface properties of titanium dioxide nanoparticles in soil solutions, Environ. Sci.: Nano 11 (2024) 1204.
[41] S.M. Kanan, C.P. Tripp, An infrared study of adsorbed organophosphonates on silica: a prefiltering strategy for the detection of nerve agents on metal oxide sensors, Langmuir 17 (2001) 2213.
[42] U. Biapo, V. Keller, P. Bazin, T. Cottineau, Investigation of interactions between organophosphorus compounds and TiO2 modified microcantilevers for molecule detection in air, Mater. Adv. 3 (2022) 3600.

[43] C.N. Rusu, J.T. Yates Jr., Adsorption and decomposition of dimethyl methylphosphonate on TiO2, J. Phys. Chem. B 104 (2000) 12292.
[44] J. Henych, V. Stengl, A. Mattsson, J. Tolasz, L. Osterlund, Chemical warfare agent simulant DMMP reactive adsorption on TiO2/graphene oxide composites prepared via titanium peroxo-complex or urea precipitation, J. Hazard Mater. 359 (2018) 482.
[45] R. Vercauteren, C. Gevers, J. Mahillon, L.A. Francis, Design of a porous silicon biosensor: characterization, modeling, and application to the indirect detection of bacteria, Biosensors 14 (2024) 104.
[46] R.M. Crooks, H.C. Yang, L.J. McEllistrem, R.C. Thomas, A.J. Ricco, Interactions between self-assembled monolayers and an organophosphonate Detailed study using surface acoustic wave-based mass analysis, polarization modulation-FTIR spectroscopy and ellipsometry, Faraday Discuss 107 (1997) 285.
[47] J.A. Moss, S.H. Szczepankiewicz, E. Park, M.R. Hoffmann, Adsorption and photodegradation of dimethyl methylphosphonate vapor at TiO2 surfaces, J. Phys. Chem. B 109 (2005) 19779.
[48] N. Rouvière, J.P. Brach, T. Honnecker, K. Christoforidis, D. Robert, V. Keller, UiO-66/TiO_2 nanostructures as adsorbent/photocatalytic composites for air treatment towards dry dimethyl methylphosphonate-laden air flow as a Chemical Warfare Agent analog, Catal. Today 413 (2023) 113960.
[49] T.N. Obee, S.J. Satyapal, Photocatalytic decomposition of DMMP on Titania, Photochem. Photobiol.: Chemistry 118 (1998) 45.
[50] A. Ahrens, M. Allers, H. Bock, M. Hitzemann, A. Ficks, S. Zimmermann, Detection of chemical warfare agents with a miniaturized high-performance drift tube ion mobility spectrometer using high-energetic photons for ionization, Anal. Chem. 94 (2022) 15440.